Exponential Variational Integrators Using Constant or Adaptive Time Step

Odysseas Kosmas and Dimitrios Vlachos

Abstract In this book article, at first we survey some recent advances in variational integrators focusing on the class of them known as exponential variational integrators, applicable in finite dimensional mechanical systems. Since these integrators are based on the space and time discretization, we start with a brief summary of the general development of the discrete mechanics and its application in describing mechanical systems with space-time integration algorithms. We, then, make an attempt to treat briefly in depth only the particular topic of adaptive time step exponential variational integrators. To this aim, the action integral along any curve segment is defined using a discrete Lagrangian that depends on the endpoints of the segment and on a number of intermediate points of interpolation. This Lagrangian is then, at any time interval, written as a weighted sum of the Lagrangians corresponding to a set of the chosen intermediate points to obtain high order integrators. The positions and velocities are interpolated here using special exponential functions. Finally, we derive exponential higher order variational integration methods for the numerical integration of systems with oscillatory solutions. The obtained exponential variational integrators using constant or adaptive time step are tested for the numerical solution of several problems showing their good behavior to track oscillatory solutions. Furthermore, we use the space-time geodesic approach of classical mechanics to explore whether the new methodology may be effective in adaptive time schemes.

O. Kosmas
Modelling and Simulation Centre, MACE, University of Manchester, Manchester, UK
e-mail: odysseas.kosmas@manchester.ac.uk

D. Vlachos (✉)
Department of Informatics & Telecommunications, University of Peloponnese, Tripoli, Greece
e-mail: dvlachos@uop.gr

A. M. Raigorodskii, M. Th. Rassias (eds.), *Discrete Mathematics and Applications*,
Springer Optimization and Its Applications 165,
https://doi.org/10.1007/978-3-030-55857-4_10

1 Introduction

During the last decades, there have been developed several numerical integration methods for Lagrangian systems, where the integrator is derived by discretizing the Hamilton's principle. This class of integration methods is known as discrete variational integrators and have specific advantages that make them attractive for many applications in mechanical systems. They are appropriate for both conservative and nearly dissipative (forced) systems. The conservative nature of variational integrators can allow substantially more accurate simulations at lower cost [1].

By understanding the geometry of space one may choose better discretizations while by understanding the geometric viewpoint one may recover the symmetries and invariants of the physical system (conservation of energy, conservation of linear and angular momentum, variational principles, etc.) [2–4].

In numerical solution of ordinary differential equations, one of the most difficult problems is related to the development of integrators for highly oscillatory systems [1]. As is well known, standard numerical schemes may require a huge number of time steps to track the oscillations. But, even with small size steps they may alter the dynamics, unless the chosen method has specific advantages. A useful category of them is that of geometric integrators, numerical schemes that preserve some geometric features of the dynamical system. These integrators provide to simulations longer time running without spurious effects (like bad energy behavior of conservative systems) than the traditional ones [5–7].

These methods are automatically symplectic thanks to the resulting good energy behavior. Also the symmetries of the discrete Lagrangian lead to conservation of orbital and angular momenta by the integrator.

In the class of asynchronous variational integrators (AVI) a refinement was developed that uses different time steps at different points in space and particularly in regions where the specific problem requires more (or less) accuracy (see [8]). The AVI are based on space-time discretizations which allow different time steps for different elements in a finite element mesh.

So far, in order to improve the numerical integration of highly oscillatory problems, e.g. [1], and derive methods as well as error bounds for families of quadrature methods that use for the required derivatives the finite difference approximations, special techniques have been developed. Alternatively, the use of the phase-lag property of [9], trigonometric fitting, and phase-fitting techniques lead to methods based on variable coefficients that depend on the characteristic frequency of the problem [10]. The latter, is known as exponential (or trigonometric) fitting and has been formulated long ago [9, 11, 12]. Exponentially fitting algorithms are considered as natural extensions of the classical polynomial fitting due to their characteristic property to approach the classical ones because the involved dominant frequencies tend to zero. The important problem of convergence of exponentially fitted methods, especially of the known as multi-step ones, has been investigated within Lyche's theory [12] (for a comprehensive discussion the reader is referred to [9]).

The main benefits of the variational integrators and phase fitting are exploited in previous works [13–15] for Lagrangian problems similar to that employed for testing ordinary differential equations (the harmonic oscillator with a given frequency ω). Furthermore, the exponential variational integrators, which solve exactly the test system, have been applied to general Lagrangian problem of single particle motion (the planar two-body problems) by determining the frequency ω at every step of the integration.

In recent years, a great number of phenomena are investigated with remarkably complex computer models and codes. Computational experiments, i.e., runs of these codes with various input data covering a wide range, lead to predictions (through the provided output) of several physical observables and parameters. In most of the cases the runs are computationally expensive and often our objective is the required computer experiments to be less time-consuming predictors of the output for the given data.

In solving special problems based on ordinary differential equations (ODEs) using numerical integration schemes, computational cost may be appreciably reduced by time adaptivity or using time adaptive steps [16, 17]. Admittedly, this tool possesses significant advantages with respect to the efficiency, the computational accuracy, and the ease in the implementation. The use, however, of symplectic integrators performs remarkably well in problems involving Hamiltonian integrations [7, 18, 19].

Many authors have, so far, addressed various derivations and have adopted symplectic integrators with variable time steps, despite the fact that the early results were not really promising [20–22]. Essentially, two main types of time variation steps have been utilized. In the first, the time step was explicitly varied in the flow of the time, a mostly problematic choice, while in the second, the time step was adopted while using the dynamical variables of the system (particle positions q, corresponding momenta p, etc.). For the case of the variable time, the derived equations are no longer in canonical Hamiltonian form leading to rather unreliable results.

Adaptive time step integrators may reduce some of the aforementioned shortcomings with high order non-symplectic schemes. Those are recently adopted [17, 23].

In improving the Galerkin type high order integrators [13–15], in such a way that adaptive time stepping to be used, the combination of space-time [16, 18] and geodesic view point of [24, 25] approaches are considered. These provide the possibility to overcome various problems that appear when symplectic integrators with variable time steps are employed. One can derive an optimal time step adaptation method computationally cheaper as much as possible.

Towards this end, a general formulation to derive high order variational integrators is presented (Section 2). They are tested on the numerical solution of some examples of the general N-body problem. In connection to those integrators we formulate the combined space-time and geodesic ideas of adaptive time stepping (Section 4) which we use to derive the proposed schemes (Section 5) and test (Section 6) in a couple of numerical applications. Finally, the advantages of the derived method are summarized in Section 7.

2 The Advantages of Variational Integrators

High order variational integrators that are applicable to physical systems where the Lagrangian is of separable form, are derived by following similar steps to those followed in the discrete variational calculus, see e.g. [4]. Thus, for a smooth and finite dimensional configuration manifold Q, one defines the discrete Lagrangian L_d through the mapping

$$L_d : Q \times Q \to \mathbb{R}. \tag{1}$$

This Lagrangian may be considered as an approximation of a continuous action obtained as

$$L_d(q_k, q_{k+1}, h_k) \approx \int_{t_k}^{t_{k+1}} L(q, \dot{q}) dt. \tag{2}$$

Then, one defines also the action sum S_d as

$$S_d : Q^{N+1} \to \mathbb{R}, \tag{3}$$

($N \in \mathbb{N}$), that corresponds to the above Lagrangian as

$$S_d(\gamma_d) = \sum_{k=0}^{N-1} h_k L_d(q_k, q_{k+1}, h_k), \tag{4}$$

where $\gamma_d = (q_0, \ldots, q_N)$ denotes the discrete trajectory of the studied system. Following the procedure of the continuous Mechanics we can further compute the derivative of L_d as

$$dL_d(q_0, q_1) = D_1 L_d(q_0, q_1) + D_2 L_d(q_0, q_1), \tag{5}$$

interpreting $D_i L_d$ as the derivative with respect to the i-argument of L_d. According to the discrete variational principle, the solutions of the discrete system are determined from the L_d. Thus, in order to obtain the equation describing the motion of the system, we extremize the action sum S_d, over all the intermediate points of the trajectory γ_d by keeping the endpoints q_0 and q_N fixed. The resulting system of difference equations are

$$h_{k-1} D_2 L_d(q_{k-1}, q_k, h_{k-1}) + h_k D_1 L_d(q_k, q_{k+1}, h_k) = 0, \tag{6}$$

where $k = 1, \ldots, N-1$. These equations are known as discrete Euler–Lagrange equations [4, 13].

To derive high order methods addressed in this work, we approximate the action integral along the curve segment with endpoints q_k and q_{k+1} (see Figure 1), we use a discrete Lagrangian that depends only on the chosen endpoints, see Equation (2).

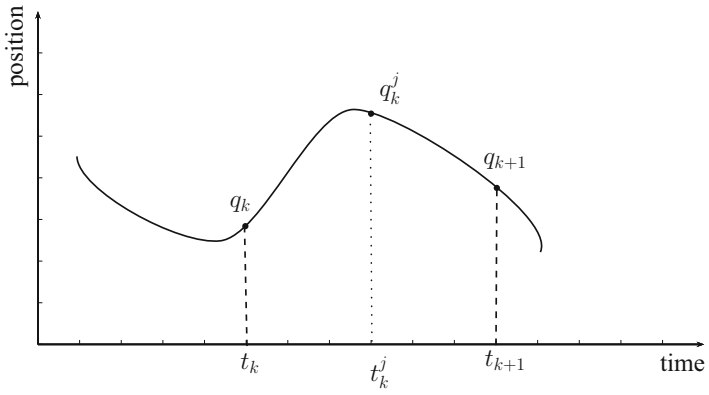

Fig. 1 Intermediate time nodes $t_k^j \in [t_k, t_{k+1}]$ and corresponding configurations q_k and q_{k+1}

This way, we obtain expressions for the configurations q_k^j and velocities $\dot{q}_k^j$ at time $t_k^j \in [t_k, t_{k+1}]$ where $j = 0, \ldots, S-1$, $S \in \mathbb{N}$. Then, by expressing the t_k^j as

$$t_k^j = t_k + C_k^j h_k \qquad \text{for} \qquad C_k^j \in [0, 1] \tag{7}$$

such that

$$C_k^0 = 0, \qquad C_k^{S-1} = 1, \tag{8}$$

where $h_k \in \mathbb{R}$ denotes the time step, we write [13]

$$\begin{aligned} q_k^j &= g_1(t_k^j) q_k + g_2(t_k^j) q_{k+1}, \\ \dot{q}_k^j &= \dot{g}_1(t_k^j) q_k + \dot{g}_2(t_k^j) q_{k+1}. \end{aligned} \tag{9}$$

Next, for the representation of the oscillatory behavior of the solution [26–29], we choose functions of the form

$$\begin{aligned} g_1(t_k^j) &= \sin\left(u - \frac{t_k^j - t_k}{h_k} u\right) (\sin u)^{-1}, \\ g_2(t_k^j) &= \sin\left(\frac{t_k^j - t_k}{h_k} u\right) (\sin u)^{-1}. \end{aligned} \tag{10}$$

For the sake of continuity, the conditions

$$g_1(t_{k+1}) = g_2(t_k) = 0 \tag{11}$$

$$g_1(t_k) = g_2(t_{k+1}) = 1 \tag{12}$$

must be fulfilled.

It should be mentioned that, for any different choice of interpolation, we define the discrete Lagrangian L_d by a weighted sum of the form [13]

$$L_d(q_k, q_{k+1}, h_k) = \sum_{j=0}^{S-1} h_k w^j L(q(t_k^j), \dot{q}(t_k^j)), \tag{13}$$

where, as can be readily proved, it holds [13, 26]

$$\sum_{j=0}^{S-1} w^j (C_k^j)^m = \frac{1}{m+1}, \tag{14}$$

with $m = 0, 1, \ldots, S-1$ and $k = 0, 1, \ldots, N-1$.

From the above equations it becomes clear that, if the time step, h_k, is equal to $h_k = h$ at every time interval, the resulting integrator is of constant time step.

By applying the above interpolation technique in combination with the trigonometric expressions of (10) and following the phase-lag analysis of [13, 26], the parameter u entering equations (10) must be determined as $u = \omega h$. For problems involving a definite frequency ω (such as the harmonic oscillator), the parameter u can be easily computed. However, for the solution of periodic orbit problems (orbital problems) of the general N-body problem, where no unique frequency of the motion can, in general, be determined, a new parameter u must be computed by estimating the frequency of the motion for any individual moving mass of the system [14, 15].

3 Exponential Integrators

When trying to solve numerically Hamiltonian systems of the form

$$\ddot{q} + \Omega q = g(q), \qquad g(q) = -\nabla U(q), \tag{15}$$

where Ω is a diagonal matrix (it may contain diagonal entries ω with large modulus) and $U(q)$ is a smooth potential function, we mostly are interested in the long time behavior of the numerical solutions. In such cases, application of the above methods imposes ωh to be rather large. Then, because an exact discretization of Equation (15) satisfies the equation $q_{n+1} - 2\cos(h\omega)q_n + q_{n-1} = 0$, we may write

$$q_{n+1} - 2\cos(h\omega)q_n + q_{n-1} = h^2 \psi(\omega h) g(\phi(\omega h) q_n), \tag{16}$$

where the functions $\psi(\omega h)$ and $\phi(\omega h)$ are even, real-valued functions satisfying the conditions $\psi(0) = \phi(0) = 1$ [5]. The latter equations represent exponential integrators (see Appendix for some typical examples).

3.1 High Order Exponential Variational Integrators

If we apply the steps of deriving high order variational integrators (see Section 2) to the Hamiltonian system (15), the discrete Euler–Lagrange equations (6) lead to the expressions

$$q_{n+1} + \Lambda(u, \omega, h, S)q_n + q_{n-1} = h^2 \Psi(\omega h) g(\Phi(\omega h) q_n), \tag{17}$$

where

$$\Lambda(u, \omega, h, S) = \frac{\sum_{j=0}^{S-1} w^j \left[\dot{g}_1(t_k^j)^2 + \dot{g}_2(t_k^j)^2 - \omega^2 \left(g_1(t_k^j)^2 + g_2(t_k^j)^2 \right) \right]}{\sum_{j=0}^{S-1} w^j \left[\dot{g}_1(t_k^j) \dot{g}_2(t_k^j) - \omega^2 g_1(t_k^j) g_2(t_k^j) \right]}. \tag{18}$$

Based on the latter two expressions, we derive exponential variational integrators that use the configurations q_k^j and velocities $\dot{q}_k^j$ of (9). We then get

$$\Lambda(u, \omega, h, S) = -2\cos(\omega h). \tag{19}$$

Whenever the latter equation holds, exponentially fitted methods relying on phase fitted variational integrators can be derived [13] which means that high order variational integrators can be considered as exponential integrators. Several numerical applications of this type have been carried out [13–15] and, due to their importance, in Section 3.3 we examine them in more detail through some representative examples.

3.2 Estimation of Frequency in Three Dimensional Particle Motions

Recently, exponential variational integrator techniques have been used [13] by estimating the required frequency on the basis of the frequency ω of a harmonic oscillator. In solving the orbital N-body problem by using a constant time step, a new way of frequency estimation is necessary to find it for each body (1) at the initial time t_0 and (2) at a time t_k, $k = 1, \ldots, N-1$.

Obviously, by applying the trigonometric interpolation (10), the parameter u can be chosen as $u = \omega h$, but for problems where the domain frequency ω is fixed and known (such as the harmonic oscillator) the parameter u can be easily computed. For the orbital N-body problem, where no global frequency is determined, u must be found by estimating the individual frequency of the motion of each moving point particle.

In the case of the 3-dimensional particle motion where N masses are moving in three dimensions, assuming that $q_i(t)$, $i = 1, \ldots, N$, denotes the trajectory and $\dot{q}_i(t)$ the velocity (with magnitude $|\dot{q}_i(t)|$) of the i-th particle, the corresponding curvatures can be computed from the known expressions

$$k_i(t) = \frac{|\dot{q}_i(t) \times \ddot{q}_i(t)|}{|\dot{q}_i(t)|^3}. \tag{20}$$

After a short time h, the angular displacement of the i-th mass is

$$\frac{h|\dot{q}_i(t) \times \ddot{q}_i(t)|}{|\dot{q}_i(t)|^2}, \tag{21}$$

which for the actual frequency gives

$$\omega_i(t) = \frac{|\dot{q}_i(t) \times \ddot{q}_i(t)|}{|\dot{q}_i(t)|^2}. \tag{22}$$

From (20) and (22) the well-known relation

$$\omega_i(t) = k_i(t)|\dot{q}_i(t)| \tag{23}$$

is satisfied (see also [13]).

Focusing on the many-body physical problem described via the Lagrangian

$$L(q, \dot{q}) = \frac{1}{2}\dot{q}^T M(q)\dot{q} - V(q), \tag{24}$$

($M(q)$ represents a symmetric positive definite mass matrix and V is the potential function), we write the continuous Euler–Lagrange equations as

$$M(q)\ddot{q} = -\nabla V(q). \tag{25}$$

In this system, the frequency $\omega_i(t_k)$ for the i-th body at time t_k, $k = 1, \ldots, N-1$ given by Equation (22), takes the form

$$\omega_i(t_k) = h^{-1}\frac{\left|M^{-1}(q_k)p_k \times \left(M^{-1}(q_k)p_k - M^{-1}(q_{k-1})p_{k-1}\right)\right|}{\left|M^{-1}(q_k)p_k\right|^2}. \tag{26}$$

The quantities on the right-hand side in the latter equation are the mass matrix, the configuration, and the momentum of the i-th body. The frequency $\omega_i(t_k)$, at an initial time instant t_0 (at which the initial positions are $\bar{q}_0$ and initial momenta are $\bar{p}_0$), is

$$\omega_i(t_0) = \frac{\left|M^{-1}(\bar{q}_0)\bar{p}_0 \times \left(-M^{-1}(\bar{q}_0)\nabla V(\bar{q}_0)\right)\right|}{\left|M^{-1}(\bar{q}_0)\bar{p}_0\right|^2}. \tag{27}$$

Equations (26) and (27) provide an "estimated frequency" for each mass in the general periodic motion of the N-body problem and allow the derivation of high order variational integrators based on trigonometric interpolation in which the frequency is estimated at every time step of the integration procedure. Compared to methods which employ constant frequency, the latter integrators show better energy behavior, i.e., smaller oscillation amplitude of the total energy is obtained [13, 14]. Before closing this section, it should be mentioned that, the linear stability of the above method is comprehensively analyzed in previous works [13, 14, 30].

3.3 Examples of Constant Time Step Exponential Integrators

Focusing on the numerical solution of the orbital problem of N-bodies moving in the gravitational field, we write the Lagrangian function as [5, 6]

$$L(q,\dot{q}) = \frac{1}{2}\sum_{i=1}^{N} m_i \dot{q}_i^2 + \sum_{i=1, j=1, i\neq j}^{N} G\frac{m_i m_j}{||q_i - q_j||}t \tag{28}$$

(G denotes the gravitational constant). In this section we study the motion of (1) the planar two-body problem and (2) that of the multi-body solar system and test the performance of the above mentioned novelties on these two systems.

3.3.1 Planar Two-Body Problem

As a first test of the above technique, we study the motion of the simple system of two objects that interact with each other through a central potential. The most famous example of this system is the planar Kepler's problem in which two masses attract each other with the gravitational force. In the solar system, such an interaction leads to elliptic orbits for the Sun–planet system and hyperbolic orbits for the Sun–comet system.

By choosing the heavier body as the center of the coordinate system, the motion remains planar. Denoting the position of the second body by $q = (q_1, q_2) \in \mathbb{R}^2$, the system's Lagrangian (28) takes the simple form

$$L(q,\dot{q}) = \frac{1}{2}\dot{q}^2 + \frac{1}{|q|}. \tag{29}$$

(for simplicity, the masses of the bodies and the gravitational constant are considered equal to 1). Also, as initial conditions we assume

$$q = (1-\epsilon, 0) \qquad \text{and} \qquad \dot{q} = \left(0, \sqrt{\frac{1+\epsilon}{1-\epsilon}}\right), \tag{30}$$

where $\epsilon \in \mathbb{R}$ is the eccentricity of the orbit [5].

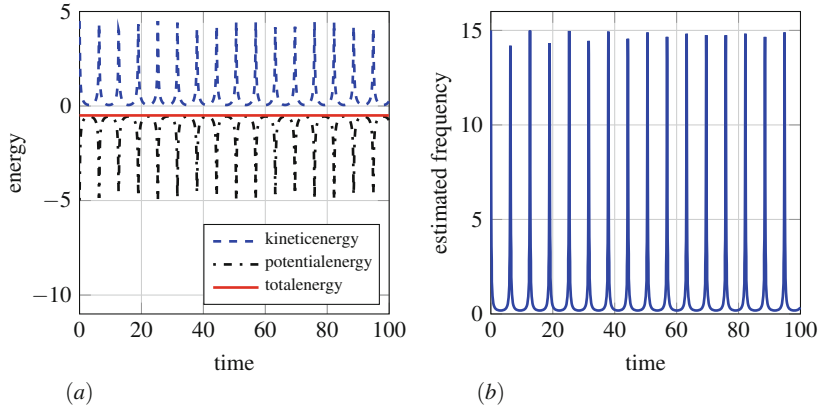

Fig. 2 Planar two-body problem with eccentricity $\epsilon = 0.8$, time step $h = 0.01$, and order of the method $S = 5$ for 10^4 steps. (**a**) Energy evolution using trigonometric interpolation. (**b**) The estimated frequency for the moving mass using the expression (22)

In trying to solve numerically the above problem, a difficulty arises when the eccentricity of the elliptical orbit is high. For example, some periodic comets have eccentricities between $0.7 \leq \epsilon \leq$ just below 1 (e.g., for Neptune's third largest moon Nereid $\epsilon = 0.750$, Halley's comet has $\epsilon = 0.967$, etc.). For this reason, we have chosen to test the above methods in the description of elliptical orbital problems with very high eccentricities for the two cases described below.

(i) In the first computational experiment, we consider the eccentricity $\epsilon = 0.8$ and we choose time step $h = 0.01$. We use trigonometric interpolation with $u = \omega h$ and $S = 5$. The good energy behavior of the method, obtained for a simulation of 10^4 steps, is illustrated in Figure 2a. The frequency is estimated at every integration step through the application of (22)–(26). The time variation is shown in Figure 2b where the peaks represent the estimated frequency at points close to the perihelion (the point where the moving mass is nearest to the central body). A comparison of the total energy evolution using constant (dashed line) and estimated (solid line) frequency is shown in Figure 3. As can be seen, even for small eccentricities ($\epsilon = 0.2$) the amplitude of the energy oscillation is smaller when the frequency is estimated at every time step of the integration process. Similar results are obtained for higher eccentricities.

(ii) In the next simulation experiment, we integrate the two-body problem in the cases of elongated orbits with the high eccentricities: $\epsilon = 0.6$, $\epsilon = 0.7$, and $\epsilon = 0.8$ and 10^3 time steps in order to explore the need of using high order variational schemes. For this reason, we test the long term behavior of two methods, the trigonometric and the Störmer–Verlet method [5], which is also variational, but of second order accuracy. For both methods, the results for the configuration q_k of the body's orbit are illustrated in Figure 4. These results demonstrate the excellent behavior of the higher accuracy method, even for

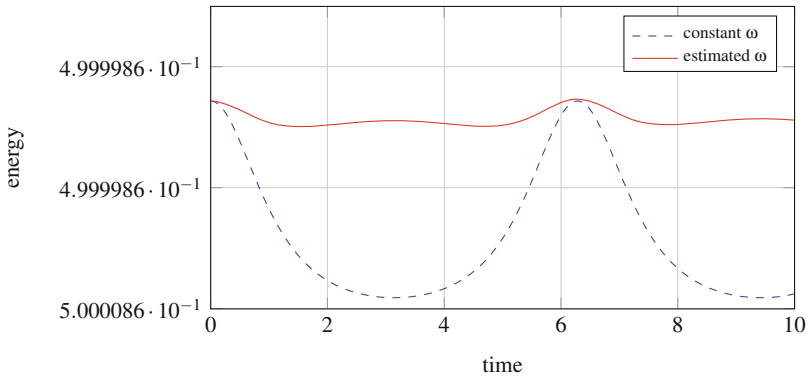

Fig. 3 Planar two-body problem with $\epsilon = 0.2$ using trigonometric interpolation for $S = 5$, $h = 0.01$. Evolution of the total energy for constant and estimated frequency using (22)

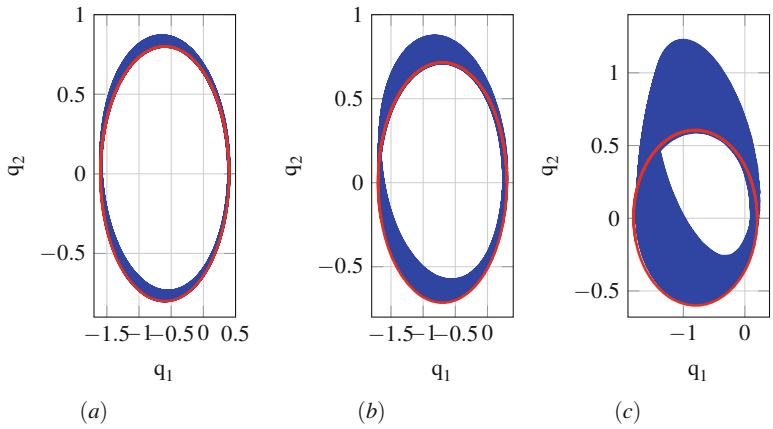

Fig. 4 Planar two-body problem for $h = 0.01$ for 10^3 steps for eccentricities (**a**) $\epsilon = 0.6$, (**b**) $\epsilon = 0.7$ and (**c**) $\epsilon = 0.8$. Long term behavior of the Störmer–Verlet method of [5] and the one that uses trigonometric interpolation with $S = 5$

orbits with extremely high eccentricity and large number of periods. On the other hand, the Störmer–Verlet method gives perturbed orbits even for small eccentricities, showing the necessity of employing higher order schemes.

3.3.2 The Modified Solar System

For multi-body systems, the advantages of choosing the parameter u via the frequency estimation of Equation (22) are illustrated by adopting the modified solar system with two planets [5]. For this system, which is described by the Lagrangian

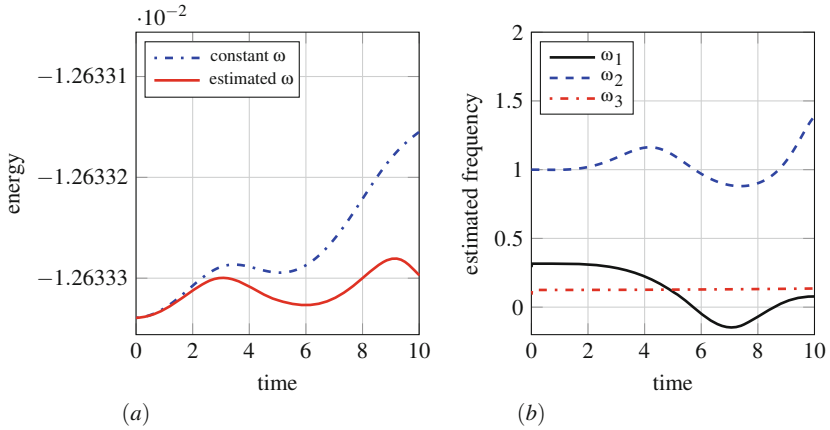

Fig. 5 Modified solar system with $h = 0.01$ and $S = 3$. (**a**) Total energy evolution using trigonometric interpolation for constant ω_i (blue line) and estimated ω_i at every time step (black line). (**b**) Estimated frequency for the three bodies of the modified solar system using the expression (22)

function (28) with $N = 3$, we choose $m_1 = 1, m_2 = m_3 = 10^{-2}$ and assume initial configurations and velocities given by

$$q_1 = (0, 0),\ q_2 = (1, 0),\ q_3 = (4, 0) \tag{31}$$

$$\dot{q}_1 = (0, 0),\ \dot{q}_2 = (0, 1),\ \dot{q}_3 = (0, 0.5). \tag{32}$$

The resulted motion of the two planets is nearly circular with periods equal to $T_1 \approx 2\pi$ and $T_2 \approx 14\pi$, respectively [5].

At first, we compare the results of (i) a variational integrator using trigonometric interpolation with constant frequencies, ω_i, $i = 1, 2, 3$, during the integration procedure, with those of (ii) a variational integrator derived by estimating the parameter u at every time step using Equation (22). In Figure 5a, we plot the total energy resulting from these two methods. The advantage of the second method at every step is obvious. In Figure 5b the evolution of the estimated angular velocities for each body (ω_1, ω_2, and ω_3, respectively) is shown.

For both numerical tests, the number of intermediate points is $S = 3$ while the time step is $h = T_1/365 = 2\pi$, i.e., equal to the period of the first planet.

4 Derivation of Time Adaptive Integrators Through the Geodesic Approach

When one studies the discrete Euler–Lagrange equation and geodesics, the main concern is how to find the equations of motion of a particle restricted to a particular curved surface (a sphere, a torus, etc.). As is well known, if a particle is constrained

to move on a particular surface, it would follow the path of a geodesic on that surface. For example, on a sphere, it would follow a great circle in its motion. The more general problem related to this issue is how to model the trajectory of a particle constrained to move on a manifold M (or simply surface) in the discrete mechanics on the basis of geodesic approach. In general, to illustrate the algorithm performance on manifolds one, for example, may compute minimal geodesics, shortest paths on a sphere, a torus, etc. and also test the computation of equidistance curves, as well as shortest paths and geodesic distances on synthetic (complicated) objects.

In many physical applications, for the numerical solutions of the governing ordinary differential equations, the class of integration schemes based on adaptive time integrators perform remarkably well. The derivation of time adaptive integrators starts from the continuous Lagrangian formulation. Here, as an example, we consider physical problems described through the simple Lagrangian

$$L(x, \dot{x}) = \frac{1}{2}\dot{x}^2 - V(x), \qquad x \in \mathbb{R} \tag{33}$$

and the corresponding second order Euler–Lagrange differential equation

$$\ddot{x} = -\frac{\partial V}{\partial x}\,. \tag{34}$$

By choosing the initial conditions as $x_0 = x(0)$ and $\dot{x}_0 = \dot{x}(0)$, an expression of $x(t)$ can be determined and adopted for some time interval $t \in [0, T]$, as a solution of (34).

We then write down the generalized Lagrangian

$$\tilde{L} = \frac{1}{2}x'^2 + \frac{1}{2V}t'^2, \tag{35}$$

where, in order to disentangle from dots representing time derivatives, the primes denote differentiation with respect to some parameter λ [25] assuming that $t = t(\lambda)$ and, thus, $x = [t(\lambda)]$. For the latter Lagrangian the corresponding Euler–Lagrange equations and the relevant initial conditions take the form

$$x'' = -\frac{1}{2V^2}\frac{\partial V}{\partial x}t'^2, \quad x_0 = x(0), \quad x_0' = \dot{x}_0 t_0' \tag{36a}$$

$$t'' = \frac{1}{V}\frac{\partial V}{\partial x}t'x', \qquad t_0 = 0, \qquad t'(0) = \alpha V(x_0). \tag{36b}$$

It is worth mentioning that, even though $\tilde{L}$ depends upon V and couples the space and time variables in a non-trivial manner, the evolution equations for x depend only on $\partial V/\partial x$. Furthermore, we note that one could add on V any constant without changing the x-dynamics [24, 25].

We now consider two functions of the parameter λ, namely $\tilde{x}(\lambda)$ and $t(\lambda)$, that are further assumed to be solutions of equations (36) for some time interval $\lambda \in [0, \tilde{T}]$. For these solutions we can write $\tilde{x}(\lambda) = x(2t/\sqrt{\alpha})$ as long as both sides of (36) are explicitly defined, that is, as long as the solutions for x and $\tilde{x}$ differ only by an arbitrary constant. This constant, in essence, operates just as a time rescaling [24, 25].

In exploring for appropriate expressions for $\tilde{x}(\lambda)$ and $t(\lambda)$, we adopt the two Lagrangians

$$L_1 = \sqrt{\acute{x}^2 + f(x)\acute{t}^2}, \qquad L_2 = \frac{1}{2}\left(\acute{x}^2 + f(x)\acute{t}^2\right). \tag{37}$$

The action corresponding to L_1 is invariant under arbitrary reparametrization of λ, whereas the L_2 action is only affine reparametrization invariant. This leads to Euler–Lagrange equations corresponding to L_2 and hence they are affine time reparametrization invariants.

The Euler–Lagrange equations that come out of L_1 are

$$\frac{d}{d\lambda}\left(\frac{\acute{x}}{\sqrt{\acute{x}^2 + f(x)\acute{t}^2}}\right) = \frac{\acute{t}^2}{2\sqrt{\acute{x}^2 + f(x)\acute{t}^2}}\frac{\partial f}{\partial x} \tag{38a}$$

$$\frac{d}{d\lambda}\left(\frac{f(x)\acute{x}}{\sqrt{\acute{x}^2 + f(x)\acute{t}^2}}\right) = 0. \tag{38b}$$

The later equations are also reparametrization invariants with respect to λ, i.e., they are invariant under the replacements $\lambda = \lambda(\mu)$ and $d\lambda/d\mu \neq 0$. This means that, a solution of (38) defines a curve in the space (x, t). Furthermore, this solution gives us information on which curve does it belong, but it does not show us the exact point at that curve. The curve in question acts as a geodesic information for the system of equations as well as for its solution. The later equations are then considered to be evolution equations, which provide us with, not only the shape of the curve, but also with its parametrization [25].

5 Time Adaptive Exponential Variational Integrators

In this section we apply the steps followed in Section 2, in the Lagrangians L_1 and L_2 of equations (37). Using (13), for the length action given by L_1, the corresponding discrete Lagrangian reads [24, 29]

$$L_{1d}(q_k, q_{k+1}, h_k) = \sum_{j=0}^{S-1} h_k w^j \sqrt{\left(\acute{x}_k^j\right)^2 + f\left(x_k^j\right)\left(\acute{t}_k^j\right)^2}, \tag{39}$$

where the x_k^j are defined using (9) and $\acute{x}_k^j$, $\acute{t}_k^j$ using the expression [29]

$$\acute{q}_k^j = \frac{\partial q_k^j}{\partial \lambda} = \frac{\partial t}{\partial \lambda}\left(\dot{g}_1(t_k^j)q_k + \dot{g}_2(t_k^j)q_{k+1}\right) = \dot{g}_1(t_k^j)q_k + \dot{g}_2(t_k^j)q_{k+1}. \quad (40)$$

For the Lagrangian (39), the discrete Euler–Lagrange equations (6) give the discrete analogues of (38a) as

$$\begin{aligned}
&\sum_{j=0}^{S-1} w^j \frac{h_k}{2d_{k,k-1}}\left[2\dot{g}_2(t_k^j)\left(\dot{g}_1(t_k^j)x_{k-1} + \dot{g}_2(t_k^j)x_k\right)\right.\\
&\quad \left. + \frac{\partial}{\partial x_k} f\left(g_1(t_k^j)x_{k-1} + g_2(t_k^j)x_k\right)\left(\dot{g}_1(t_k^j)t_{k-1} + \dot{g}_2(t_k^j)t_k\right)^2\right]\\
&\quad + \sum_{j=0}^{S-1} w^j \frac{h_{k+1}}{2d_{k+1,k}}\left[2\dot{g}_1(t_k^j)\left(\dot{g}_1(t_k^j)x_k + \dot{g}_2(t_k^j)x_{k+1}\right)\right.\\
&\quad \left. + \frac{\partial}{\partial x_k} f\left(g_1(t_k^j)x_k + g_2(t_k^j)x_{k+1}\right)\left(\dot{g}_1(t_k^j)t_k + \dot{g}_2(t_k^j)t_{k+1}\right)^2\right] = 0, \quad (41)
\end{aligned}$$

and of (38b) as

$$\begin{aligned}
&\sum_{j=0}^{S-1} w^j \frac{h_k \dot{g}_2(t_k^j)}{d_{k,k-1}}\left[f\left(g_1(t_k^j)x_{k-1} + g_2(t_k^j)x_k\right)\left(\dot{g}_1(t_k^j)t_{k-1} + \dot{g}_2(t_k^j)t_k\right)^2\right]\\
&\quad + \sum_{j=0}^{S-1} w^j \frac{h_{k+1}\dot{g}_1(t_k^j)}{d_{k+1,k}}\left[f\left(g_1(t_k^j)x_k + g_2(t_k^j)x_{k+1}\right)\left(\dot{g}_1(t_k^j)t_k + \dot{g}_2(t_k^j)t_{k+1}\right)^2\right] = 0.
\end{aligned} \quad (42)$$

In the latter equation $d_{k+1,k}$ is given by [29]

$$\begin{aligned}
d_{k+1,k} = \Bigg\{&\left[\dot{g}_1(t_k^j)x_k + \dot{g}_2(t_k^j)x_{k+1}\right]^2\\
&+ f\left(g_1(t_k^j)x_{k-1} + g_2(t_k^j)x_k\right)\left[\dot{g}_1(t_k^j)t_{k-1} + \dot{g}_2(t_k^j)t_k\right]^2\Bigg\}^{\frac{1}{2}}
\end{aligned} \quad (43)$$

and $d_{k,k-1}$ by

$$\begin{aligned}
d_{k,k-1} = \Bigg\{&\left[\dot{g}_1(t_{k_1}^j)x_{k-1} + \dot{g}_2(t_{k-1}^j)x_k\right]^2 +\\
&f\left(g_1(t_{k-1}^j)x_{k-2} + g_2(t_{k-1}^j)x_{k-1}\right)\left[\dot{g}_1(t_{k-1}^j)t_{k-2} + \dot{g}_2(t_{k-1}^j)t_{k-1}\right]^2\Bigg\}^{\frac{1}{2}}.
\end{aligned} \quad (44)$$

In accordance with the continuous formulation, Equations (41) and (42) are not independent. To solve the above system, we can choose arbitrary step sizes in either time t or space x direction and solve these equations for the x or t, respectively.

Once the discrete Euler–Lagrange equations (41) and (42) are solved, we get a sequence of points $(x_0, t_0), \ldots, (x_N, t_N)$, where $t_0, \ldots, t_N$ does not necessarily represent the physical time. Using this sequence of points, for the discrete Hamiltonian we may write [24, 25]

$$H_d(x_0, x_1, h_0) = -h_0 D_3 L_d(x_0, x_1, h_0) - L_d(q_0, q_1, h_0)\,. \tag{45}$$

Recalling that the energy of the system, expressed by its Hamiltonian, is the conjugate variable of the physical time, i.e.,

$$H_d(x_0, x_1, h_0) = H_d(x_1, x_2, h_1), \tag{46}$$

we can restore the physical time.

6 Numerical Results

In this section, we apply the above time adaptive exponential variational integrators in the following systems: (1) the simple pendulum and (2) the orbital two-body problems with extremely high eccentricities of their periodic orbits.

6.1 Harmonic Oscillator

The numerical scheme derived in Section 5 is tested below in the case of a simple pendulum described through the (approximate) Lagrangian

$$L(q, \dot{q}) = \frac{1}{2}\dot{q}^2 - \frac{1}{2}\omega^2 q^2, \tag{47}$$

leading to the equation of motion

$$\ddot{q} = -\omega^2 q. \tag{48}$$

Using the interpolation of (9), the discrete Lagrangian that provides the system's equations of motion takes the form

$$L_d(q_k, q_{k+1}) = \frac{h}{2}\left[\sum_{j=0}^{S-1} w^j \left(\dot{g}_1(t_k^j)q_k + \dot{g}_2(t_k^j)q_{k+1}\right)^2 - \omega^2 \sum_{j=0}^{S-1} w^j \left(g_1(t_k^j)q_k + g_2(t_k^j)q_{k+1}\right)^2\right]. \tag{49}$$

For the latter Lagrangian, following Section 5, the discrete Euler–Lagrange equations provide the two-step variational integrator [15, 28]

$$q_{k+1} + \frac{\sum_{j=0}^{S-1} w^j \left[\dot{g}_1(t_k^j)^2 + \dot{g}_2(t_k^j)^2 - \omega^2\left(g_1(t_k^j)^2 + g_2(t_k^j)^2\right)\right]}{\sum_{j=0}^{S-1} w^j \left[\dot{g}_1(t_k^j)\dot{g}_2(t_k^j) - \omega^2 g_1(t_k^j) g_2(t_k^j)\right]} q_k + q_{k-1} = 0. \tag{50}$$

In order to demonstrate the benefits of the latter integrator on the numerical accuracy of the obtained methods, we compare its performance in the following two cases: (1) in the methods adopting constant time step (see Section 2) and (2) in the methods proposed in Section 5 (adaptive time step methods). We check the energy error at a specific integration time $t = 3$ (arbitrary taken) for five different frequencies $\omega \in \{1, 5, 10, 15, 20\}$ and initial conditions $(q_0, p_0) = (2, 1)$, see Figure 6. As can be seen both methods increase the energy error as the frequency of the problem increases. Secondly, even though for relatively small values of $\omega < 5$ both methods lead to energy error smaller than about 10^{-11}, for high frequency values, constant time step schemes lead to clearly larger energy error.

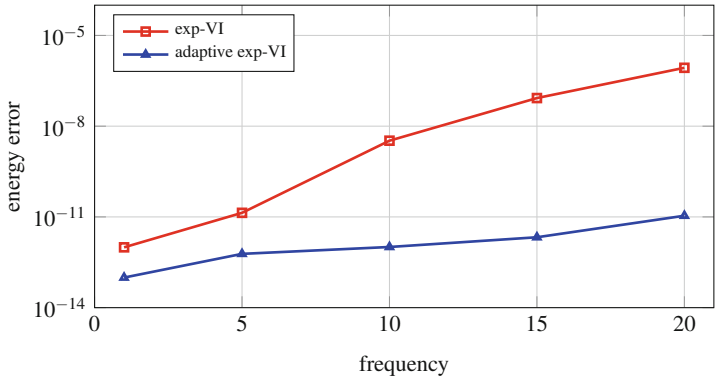

Fig. 6 Energy error for the harmonic oscillator using trigonometric interpolation (Section 2) versus the time adaptive one (Section 5) for the frequencies $\omega = 1$, $\omega = 5$, $\omega = 10$, $\omega = 15$, and $\omega = 20$

In computing the above results, both methods were considered to be third order methods, i.e., $S = 4$, while similar results have been obtained for other choices of S. We should also note that, we have chosen the same initial time step $h = 0.05$ for all results of Figure 6.

In order to illustrate how the specific choice of the time step affects significantly the computational cost, a prominent concept for our present work, we consider below some more complicated examples.

6.2 *Orbits of the Two-Body Problem with Extremely High Eccentricities*

To check the efficiency of the proposed technique, we consider again the Kepler's two-body problem discussed in Section 3.3.1 but now in the case of periodic orbits with remarkably high eccentricities (just below unity, $\epsilon = 0.99$). We compare the performance for long term integrations (10^6 periods) of the methods of Section 2 with that of the methods of Section 5. Figure 7 shows the exact orbit obtained with the method of Section 2 (solid line), the calculated points for the first period (points labeled with ∘) and the calculated points for the last period (points labeled with □). While most of the standard symplectic schemes (among them the one discussed in Section 2) fail to track the periodic orbit for such a high eccentricity, see [17], when adaptive time step is utilized, the obtained integrator is extremely stable, keeping the orbit close to the exact one. For this numerical experiment the observed energy error is oscillating around much smaller amplitude values (around 10^{-7}).

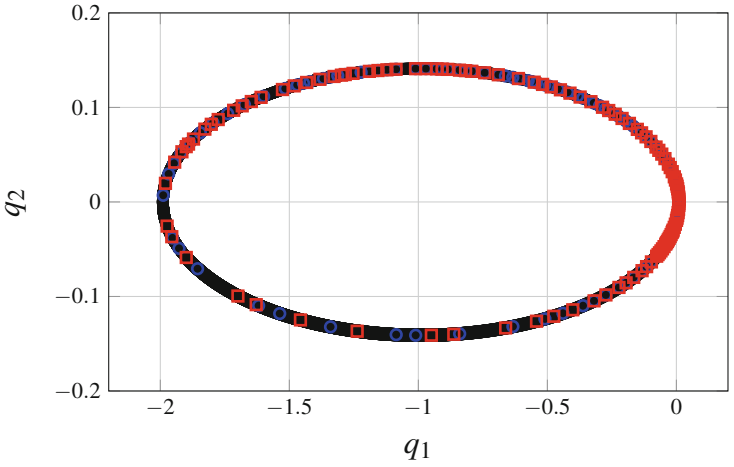

Fig. 7 Periodic orbits of the 2-body problem with eccentricity 0.99 for 10^6 periods. (1) Exact solution (solid line) and (2) calculated points for the first (open circle) and last period (open square) using the exponential variational integrators of Section 5

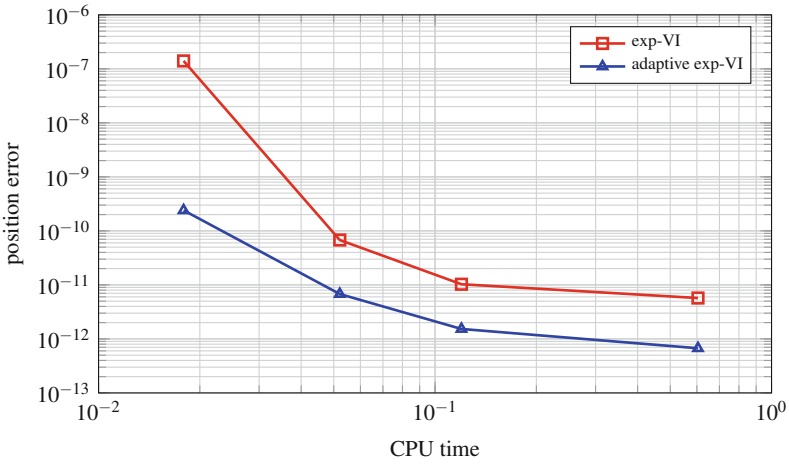

Fig. 8 Position error versus CPU time, for a 2-body problem moving in periodic orbit with eccentricity $\epsilon = 0.99$, taken at an arbitrary time $t = 3$ through numerical integration with an exponential variational integrator that uses constant time step (red line) compared to the one that uses adaptive time step (blue line)

As a final benefit of the proposed method, we explore the numerical convergence. To this aim, we choose as initial conditions the $(q_0, p_0) = (2, 2)$ and the time interval $[0, 3]$. We first calculate the global errors for the position $q(t)$ at $t = 3$ (arbitrary taken, but following [15, 31]) while using constant time steps $h \in \{0.01, 0.05, 0.1, 0.5, 1\}$. Figure 8 shows the resulting errors versus the computational time needed to obtain them (red line). It is obvious that smaller position errors are obtained for short time steps, which leads to longer computational time. When the adaptive time step exponential integrator of Section 5 is applied (blue line), the position error obtained is remarkably smaller. It should be mentioned that, in obtaining these results, we forced the proposed schemes to take the same computational time with that taken when constant time step is applied.

7 Conclusions

In this article, at first we reviewed briefly the concepts and relevant literature in discrete Lagrangian Mechanics and specifically in the discrete variational integrators developed the last decades for solving numerically the discrete Euler–Lagrangian equations. A great number of books and research articles published in this field is incorporated in the reference list below. These works have appreciably contributed in the development, enhancement, and enrichment of the topic of discrete variational integrators.

We have also presented a brief review on the extensions and refinements of the class of discrete exponential variational integrators with a particular regard to time adaptive exponential integrators. Focusing on systems of which the Lagrangian is of separable form, a methodology for deriving high order exponential variational integrators with adaptive time step has been developed. After the above, the following concluded remarks are extracted.

1. The procedure and methodology developed unfold the standard Euler–Lagrange character to its space-time manifold and translate it through the geodesic (shortest route) connecting two points on a curved surface.
2. In contrast to all the previous extensions, from the adaptive time step methods, rather than optimizing the choice of step sizing, we introduced an artificial time step parameter, and used the energy behavior in order to calculate the actual one.
3. Specifically, the proposed methods do not need to optimize the step size and, instead, one can employ the space-time geodesic formulation to generate an adaptive scheme that still preserves general underlying geometric structure properties of the system.

Finally, it is noteworthy to mention that, simulation tests showed that, this technique integrates efficiently stiff systems (like the two-body problem with very high eccentricity up to $\epsilon = 0.99$) while conserving at the same time all the benefits of the classical variational integrators.

Acknowledgement Dr. Odysseas Kosmas wishes to acknowledge the support of EPSRC via grant EP/N026136/1 "Geometric Mechanics of Solids."

Appendix

By denoting $\mathrm{sinc}(\xi) = \sin(\xi)/\xi$, special cases of the exponential integrators described using (16) can be obtained, i.e.,

- Gautschi type exponential integrators [11] for

$$\psi(\Omega h) = \mathrm{sinc}^2\left(\frac{\Omega h}{2}\right), \qquad \phi(\Omega h) = 1$$

- Deuflhard type exponential integrators [32] for

$$\psi(\Omega h) = \mathrm{sinc}(\Omega h), \qquad \phi(\Omega h) = 1$$

- García-Archilla et al. type exponential integrators [33] for

$$\psi(\Omega h) = \mathrm{sinc}^2(\Omega h), \qquad \phi(\Omega h) = \mathrm{sinc}(\Omega h)$$

Finally, in [5] a way to write the Störmer–Verlet algorithm as an exponential integrators is presenting.

References

1. B. Engquist, A. Fokas, E. Hairer, A. Iserles, *Highly Oscillatory Problems* (Cambridge University Press, Cambridge, 2009)
2. J. Wendlandt, J.E. Marsden, Mechanical integrators derived from a discrete variational principle. Physica D **106**, 223–246 (1997)
3. C. Kane, J.E. Marsden, M. Ortiz, Symplectic-energy-momentum preserving variational integrators. J. Math. Phys. **40**, 3353–3371 (2001)
4. J.E. Marsden, M. West, Discrete mechanics and variational integrators. Acta Numer. **10**, 357–514 (2001)
5. E. Hairer, C. Lubich, G. Wanner, Geometric numerical integration illustrated by the Störmer-Verlet method. Acta Numer. **12**, 399–450 (2003)
6. B. Leimkuhler, S. Reich, *Simulating Hamiltonian Dynamics*. Cambridge Monographs on Applied and Computational Mathematics (Cambridge University Press, Cambridge, 2004)
7. S. Ober-Blöbaum, Galerkin variational integrators and modified symplectic Runge–Kutta methods. IMA J. Numer. Anal. **37**, 375–406 (2017)
8. A. Lew, J.E. Marsden, M. Ortiz, M. West, Asynchronous variational integrators. Arch. Ration. Mech. Anal. **167**, 85–156 (2003)
9. L. Brusca, L. Nigro, A one-step method for direct integration of structural dynamic equations. Int. J. Numer. Methods Eng. **15**, 685–699 (1980)
10. H. Van de Vyver, A fourth-order symplectic exponentially fitted integrator. Comput. Phys. Commun. **174**, 255–262 (2006)
11. W. Gautschi, Numerical integration of ordinary differential equations based on trigonometric polynomials. Numer. Math. **3**, 381–397 (1961)
12. T. Lyche, Chebyshevian multistep methods for ordinary differential equations. Numer. Math. **19**, 65–75 (1972)
13. O.T. Kosmas, D.S. Vlachos, Phase-fitted discrete Lagrangian integrators. Comput. Phys. Commun. **181**, 562–568 (2010)
14. O.T. Kosmas, D.S. Leyendecker, Analysis of higher order phase fitted variational integrators. Adv. Comput. Math. **42**, 605–619 (2016)
15. O.T. Kosmas, S. Leyendecker, Variational integrators for orbital problems using frequency estimation. Adv. Comput. Math. (2018). https://doi.org/10.1007/s10444-018-9603-y
16. J.E. Marsden, G.W. Patrick, S. Shkoller, Multisymplectic geometry, variational integrators, and nonlinear PDEs. Commun. Math. Phys. **199**, 351–395 (1998)
17. E. Hairer, Variable time step integration with symplectic methods. Appl. Numer. Math. **25**, 219–227 (1997)
18. C. Kane, J.E. Marsden, M. Ortiz, Symplectic energy-momentum preserving variational integrators. J. Math. Phys. **40**, 3353 (1999)
19. M. Leok, J. Zhang, Discrete Hamiltonian variational integrators. IMA J. Numer. Anal. **31**, 1497–1532 (2011)
20. R.D. Skeel, Variable step size destabilizes the Störmer/leapfrog/Verlet method. BIT Numer. Math. **33**, 172–175 (1993)
21. M.P. Calvo, J.M. Sanz-Serna, The development of variable-step symplectic integrators, with application to the two-body problem. SIAM J. Sci. Comput. **14**, 936–952 (1993)
22. J.P. Wright, Numerical instability due to varying time steps in explicit wave propagation and mechanics calculations. J. Comput. Phys. **140**, 421–431 (1998)

23. S. Reich, Backward error analysis for numerical integrators. SIAM J. Numer. Anal. **36**, 1549–1570 (1999)
24. S. Nair, Time adaptive variational integrators: a space-time geodesic approach. Phys. D Nonlinear Phenom. **241**, 315–325 (2012)
25. O.T. Kosmas, D.S. Vlachos, A space-time geodesic approach for phase fitted variational integrators. J. Phys. Conf. Ser. **738**, 012133 (2016)
26. O.T. Kosmas, S. Leyendecker, Phase lag analysis of variational integrators using interpolation techniques. Proc. Appl. Math. Mech. **12**, 677–678 (2012)
27. O.T. Kosmas, Charged particle in an electromagnetic field using variational integrators. ICNAAM Numer. Anal. Appl. Math. **1389**, 1927 (2011)
28. O.T. Kosmas, D.S. Vlachos, Local path fitting: a new approach to variational integrators. J. Comput. Appl. Math. **236**, 2632–2642 (2012)
29. O.T. Kosmas, D. Papadopoulos, Multisymplectic structure of numerical methods derived using nonstandard finite difference schemes. J. Phys. Conf. Ser. **490**, 012205 (2014)
30. O.T. Kosmas, S. Leyendecker, Stability analysis of high order phase fitted variational integrators. Proc. WCCM XI - ECCM V - ECFD VI **1389**, 865–866 (2014)
31. A. Stern, E. Grinspun, Implicit-explicit integration of highly oscillatory problems. SIAM Multiscale Model. Simul. **7**, 1779–1794 (2009)
32. P. Deuflhard, A study of extrapolation methods based on multistep schemes without parasitic solutions. Z. Angew. Math. Phys. **30**, 177–189 (1979)
33. B. García-Archilla, M.J. Sanz-Serna, R.D. Skeel, Long-time-step methods for oscillatory differential equations. SIAM J. Sci. Comput. **20**, 930–963 (1999)